SIMULATING TIME-DEPENDENT ROCKFALL INITIATION BY PROGRESSIVE SUBCRITICAL CRACK GROWTH

Zack Tuckey
Jacobs Group (Australia) Pty Ltd

https://doi.org/10.56295/AGJ6111

ABSTRACT

Progressive brittle fracture plays an important role in rockfall initiation. Although the magnitude of in situ stress near the surface of a slope may be low relative to the strength of intact rock, gravitational stresses become concentrated near the tips of pre-existing discontinuities, promoting the slow process of subcritical crack growth. Over time, subcritical crack propagation reduces the size of intact rock bridges that interrupt an incipient failure surface, increasing the stress intensity at the advancing crack front. Eventually the stress intensity reaches a critical threshold where the fracture toughness of intact rock is exceeded, causing a rapid acceleration of crack growth and sudden failure.

This paper demonstrates a modified fracture mechanics model for time-dependent subcritical crack growth, applied using the bonded block discrete element method. A series of conceptual numerical models are developed based on the geological environment of Blue Mountains National Park in New South Wales, where the Triassic sandstone formations of the Narrabeen Group outcrop in cliffs up to 200 m high. The landscape of the Blue Mountains has been shaped by stream incision and escarpment retreat processes that now are dominated by gravity-driven slope failures, including rockfalls that vary in magnitude from discrete minor block falls up to rock mass scale cliff collapse events. This investigation first explores a simplified model for progressive failure of an overhanging sandstone slab, driven by time-dependent propagation of a vertical rear release joint. The methodology is then extended to consider collapse of a sandstone cliff by undermining failure of a weaker underlying shale layer. The models demonstrate how the time required for rockfall initiation varies depending on the geometry and persistence of pre-existing discontinuities and the intact rock bridges that must fail for an incipient rockfall block to detach. When combined with empirical methods for estimating rockfall magnitude-frequency relationships, the proposed methodology can help to improve the temporal estimates of rockfall probability that form a critical input to rockfall risk assessment.

1 INTRODUCTION

Slope risk assessment requires geotechnical practitioners to develop a temporal estimate for the probability of failure. For discontinuity-controlled rockfalls, failure is frequently triggered by the sudden brittle fracture of intact rock bridges that interrupt the incipient failure surface, providing the cohesion and tensile strength that supports the rock block *in situ*. The timing of brittle failures is difficult to predict: the rockfall detachment surface may develop through a stepwise process of damage accumulation, characterised by instantaneous crack growth events followed by long periods of apparent quiescence (Donati et al., 2023). Collapse may occur suddenly, involving a rapid acceleration of crack growth once the area of the incipient release surface reaches a critical threshold. Figure 1 shows a conceptual illustration of time-dependent rock slope failure, with progressive damage accumulation and reduction in factor of safety by (1) episodic processes that cause a nearly instantaneous reduction in shear or tensile strength; and (2) slow, continuous processes that reduce rock strength through cyclical changes in stress that produce hysteretic deformation.

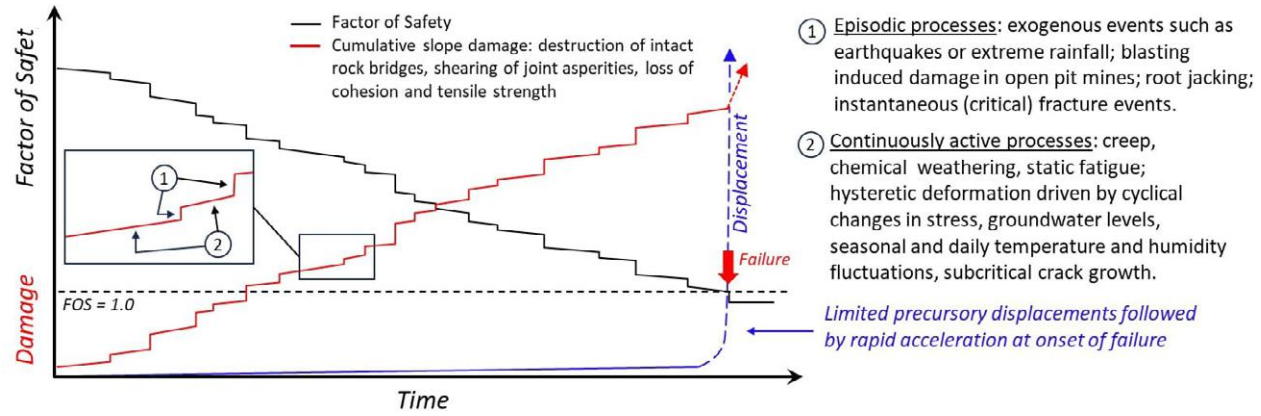

Figure 1: Conceptual illustration of time-dependent brittle slope failure (modified after Donati et al., 2023)

This investigation presents a study of time-dependent rockfall initiation based on the geological environment of Blue Mountains National Park, where the NSW National Parks and Wildlife Service (NPWS) manages an extensive trail network encompassing hundreds of kilometres of walking tracks and bushfire management trails. Some of the most popular trails are visited by hundreds of thousands of walkers each year, and many of them pass below sandstone cliffs over 200 m high. Over the last decade, landslides and rockfalls have infrequently caused serious injuries and fatalities, and more frequently caused major damage to walking tracks and fire trails. In response, NPWS has developed and published a set of landslide risk management procedures based on the quantitative risk assessment (QRA) framework of the Australian Geomechanics Society (2007).

Estimating the annualised probability of rockfall remains a key source of QRA uncertainty. This investigation demonstrates how the discrete element method can be used to simulate the time-dependent brittle failure processes that precede rockfall initiation, thereby helping to improve temporal estimates of rockfall probability. First, a series of conceptual models are developed in *UDEC* using the bonded block methodology, with a fracture mechanics model adapted from Kemeny (2005) to simulate time-dependent subcritical crack growth. The conceptual models investigate the release of a discrete overhanging sandstone slab bounded by a non-persistent vertical rear release joint. The modelling methodology is then extended to consider collapse of a sandstone cliff by undermining failure of a weaker underlying shale layer. The results demonstrate how the time required for rockfall initiation varies depending on cliff geometry, the persistence of pre-existing discontinuities and intact rock bridges, and *in situ* stress.

2 THE ROLE OF INTACT ROCK BRIDGES IN SLOPE STABILITY

For over sixty years geotechnical researchers have recognised that intact rock bridges play a crucial role in the stability of rock slopes. Terzaghi (1962) introduced the concept of coplanar or "in plane" rock bridges represented as patches of intact rock along non-persistent discontinuities. Jennings (1970) extended this concept to a limit equilibrium approach to estimate factor of safety against planar sliding, with equivalent Mohr-Coulomb cohesion and friction angle calculated based on the proportions of intact rock bridges and pre-existing discontinuity surfaces along a composite failure plane. Although Jennings' original method ignored tensile failure, Figure 2 shows how the concept of a continuity coefficient K can be adapted to the problem of an overhanging rock wedge bounded by pre-existing joints (J1 and J2) and bedding (B), where the tensile strength of intact rock bridges $\sigma_{t(eq)}$ may be expected to govern stability.

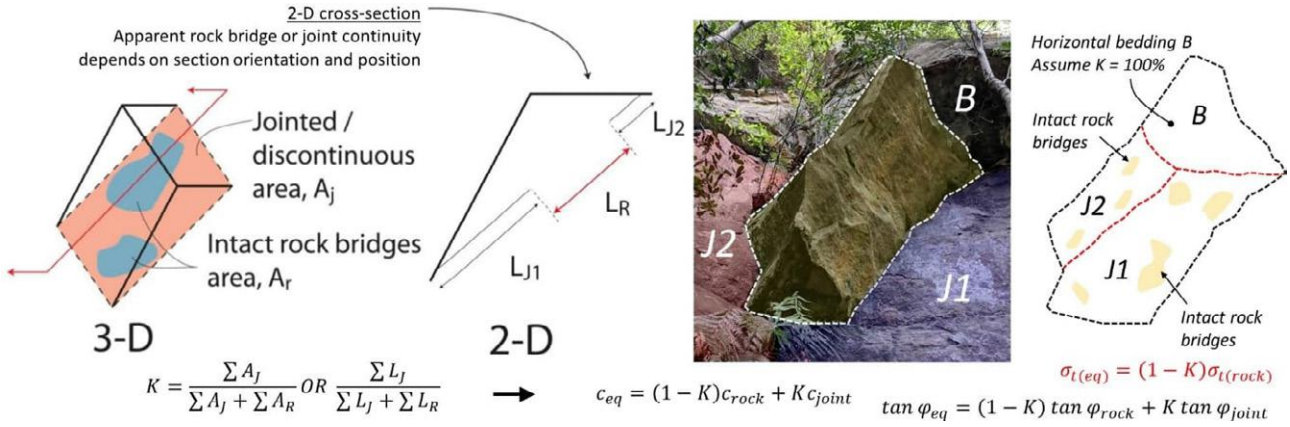

Figure 2: Conceptual illustration of coplanar intact rock bridges and example of an overhanging wedge

Early investigations into the role of rock bridges in slope stability focused on the problem of step-path failure in large open pit slopes, where an inter-ramp or overall slope scale failure surface could comprise segments of pre-existing discontinuities separated by intact rock or larger *rock mass* bridges (Baczynski, 2000). Researchers extended the Jennings-limit equilibrium approach by using statistical techniques to estimate the shear strength of many potential step-paths generated using geometry statistics for discontinuities and intact rock bridges derived from field mapping data (Call and Nicholas, 1978; McMahon, 1979; Einstein et al. 1983). Step-path shear strength statistics could then be used for probabilistic or deterministic limit equilibrium slope stability analysis. Computing advancements over the last few decades have enabled increasingly complex approaches to simulate the fracture of intact rock bridges in slopes: discrete fracture networks (DFN) can explicitly represent a rock mass fracture network (Dershowitz et al., 1998), and these DFN models can be incorporated into synthetic rock mass (SRM) numerical analyses that simulate brittle fracture using bonded particle methods (Mas Ivars et al, 2011), hybrid finite-discrete element techniques (Stead et al., 2006), finite difference and boundary element methods (Scavia, 1990), or lattice-spring models (Havaej and Stead, 2016).

Despite the development of increasingly sophisticated modelling tools, two main sources of uncertainty continue to challenge the prediction of brittle rock slope failures. First, reliable measurement of intact rock bridges may not be

possible until after failure has occurred (Elmo et al., 2018). Even for small rockfalls with simple geometry, it is not practical to directly measure intact rock bridges in the field, because they are occluded inside the rock mass. Empirical studies have measured intact rock bridge content *a posteriori* by examination of rockfall detachment scars (e.g. Paronuzzi and Serafini, 2009; Fraysinnes and Hantz, 2006). Shang et al. (2017) introduced a "forensic excavation" technique where expansive grout is injected into rock blocks along incipient discontinuities; the split discontinuity surfaces can then be inspected to measure failed rock bridges. Although these methods provide insight into rock bridge content of failed blocks, they cannot be directly extended to a predictive estimate of *in situ* rock bridge content of a stable slope. Emerging research shows that geophysical techniques including ground penetrating radar (Deparis et al., 2007) and infrared thermography (Guerin et al., 2018) may be able to provide indirect measurement of intact rock bridges under certain conditions, but these techniques have not been advanced into to accepted engineering practice.

The second challenge relates to the temporal dimension of brittle rock slope failure, which is the primary subject of this paper. Limit equilibrium methods consider that all rock bridges fail simultaneously and instantaneously. In contrast, field studies have shown that brittle rockfalls are time-dependent and progressive. For example, Collins and Stock (2016) used terrestrial LiDAR combined with crack meters, temperature, and light sensors to monitor deformation of exfoliation slabs on granite cliffs in Yosemite National Park in California, USA; they showed that daily, seasonal, and annual temperature fluctuations cause cyclic opening, closure, and propagation of incipient exfoliation joints. The daily temperature-deformation response forms hysteretic loops that result in long-term permanent deformation, which the authors propose is due to subcritical crack growth. Although numerical methods may be used to simulate progressive fracture processes, the mechanical timestep used in the solution process does not represent real time. To overcome this limitation, this investigation expands on a fracture mechanics model for subcritical crack growth first proposed by Kemeny (2003, 2005). The model is implemented with the discrete element method to simulate the time-dependent loss of cohesion and tensile strength from the progressive destruction of intact rock bridges.

3 ROCKFALL IN BLUE MOUNTAINS NATIONAL PARK

3.1 GEOLOGICAL SETTING

Blue Mountains National Park is part of a world heritage-listed conservation area spanning over one million hectares of protected wilderness on the western outskirts of Sydney. The park encompasses an uplifted tableland of Triassic sandstone that has been incised by rivers and streams, forming deep valleys surrounded by cliffs. The upper cliffs are comprised of the massive, quartzose Banks Wall Sandstone of the Narrabeen Group. The Banks Wall Sandstone is underlain by the Mount York Claystone, a marker unit of low strength, red-brown kaolinitic claystone that that forms a continuous bench in the middle of the cliffs that can be traced for kilometres across the escarpment. The lower cliffs are formed by the Burra-Moko Head Sandstone, an early Triassic quartzose to quartz-lithic sandstone that is up to 110 m thick, underlain by interbedded claystone, shales, and quartz-lithic sandstones of the Caley Formation, which forms the basal unit of the Narrabeen Group and the Permian-Triassic boundary. The late Permian Illawarra Coal Measures outcrop at the base of the cliffs, comprising coal seams, torbanite (oil shale), siltstone, and minor sandstone layers. Figure 3 shows an interpreted cross section and annotated photogrammetry image highlighting the main geological units and walking tracks that traverse across the cliffs and colluvial slopes near Wentworth Falls. Zones of geologically frequent rockfall are inferred from the presence of overhangs and pale, fresh sandstone.

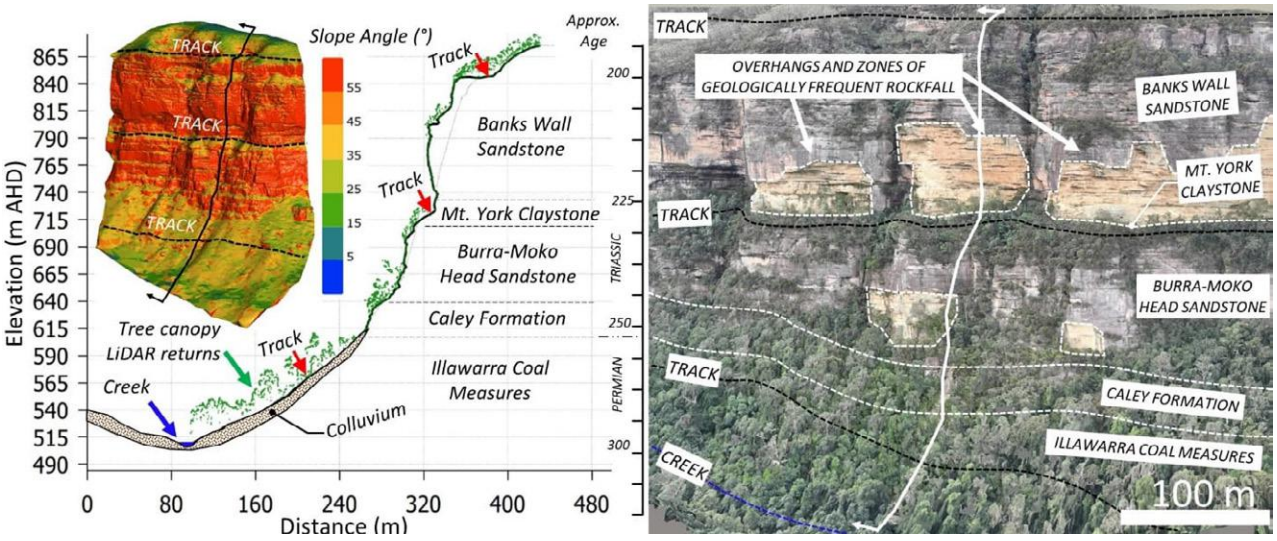

Figure 3: Interpreted LiDAR cross section and photogrammetry imagery of the cliffs near Wentworth Falls

Two orthogonal sets of high persistence vertical joints developed during the process of lithification and uplift, typically trending roughly east-west and north-south. Combined with horizontal bedding discontinuities, these joint sets provide kinematic release for rockfalls, with preferential erosion of underlying claystone producing sandstone overhangs that eventually topple or slide from the cliffs and onto the colluvial talus slopes below.

3.2 COMMON ROCKFALL FAILURE MECHANISMS

Initial uplift of the Blue Mountains occurred during the Cretaceous and this was followed by further episodes of uplift during the Cenozoic (Fergusson and Hatherly, 2023). Since approximately the late Miocene (~10 Ma) the geomorphic processes shaping the landscape have been dominated by erosion from stream incision and gravity-driven slope failures (Hatherly, 2019). Rockfalls are ubiquitous along the escarpment cliffs, being products of the long-term processes of valley incision and escarpment retreat that have produced the modern landscape. Typically, a new rockfall or landslide is reported somewhere in the park about once per month, frequently impacting popular walking tracks that connect the top of the escarpment to the valleys below by descending steep switchbacks, fabricated metal and carved stone stairways that pass directly under cliffs and overhangs.

Rockfalls in the Narrabeen Group rocks often involve failure of overhanging or undermined blocks of sandstone, with cubic to tabular blocks formed by the two main subvertical joint sets and subhorizontal bedding. Where walking tracks pass directly under natural or excavated overhangs, blocks may freefall just a few metres directly onto the track; other recorded rockfalls have involved long runout of blocks onto tracks that traverse the valley slopes below the cliffs. Figure 4 shows selected examples of overhanging sandstone blocks where stability is inferred to be influenced by the presence of intact rock bridges. Rockfall initiation may be promoted by tree root jacking, elevated pore pressures from intense rainfall events, or may occur with no obvious external trigger, as the culmination of slow, long-term subcritical crack growth driven by gravitational loading under self-weight.

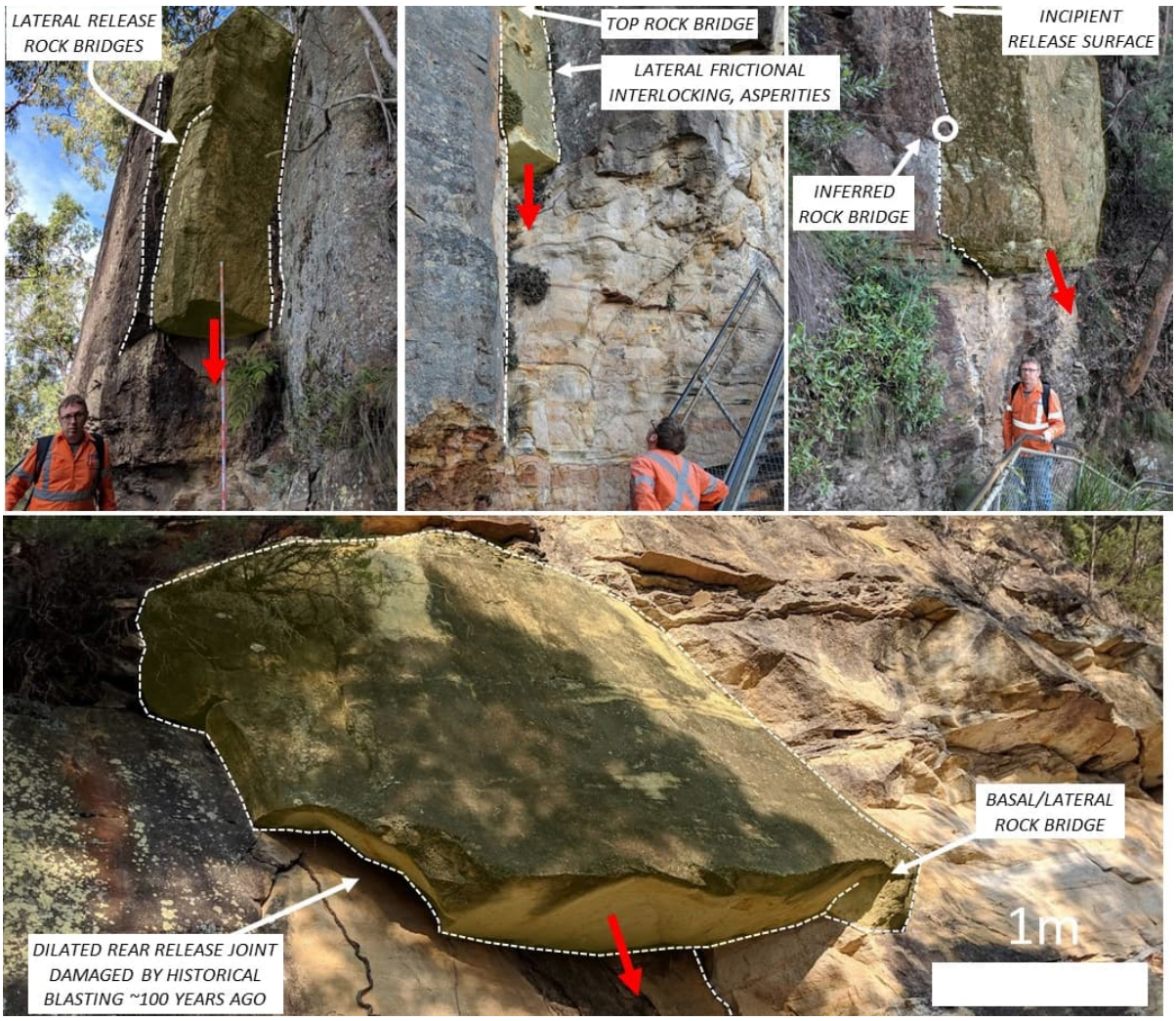

Figure 4: Examples of potential rockfall blocks involving propagation of vertical joints

The development of sandstone overhangs is promoted by the preferential erosion of weak shale and claystone layers that degrade with cyclical changes in moisture content. As the weaker horizon is eroded, the overhang depth increases, promoting extensile strains in the rock mass above, causing subvertical joints to dilate and tilting the overlying sandstone rock mass towards the valley below. In some cases, this preferential erosion has been accelerated by deliberate excavation of shale or claystone layers during the construction of walking tracks in the early 1900s. After the rear release joints have fully propagated, the eventual collapse may involve rotational toppling, or time-dependent bearing capacity failure of the eroding shale or claystone layer (Figure 5).

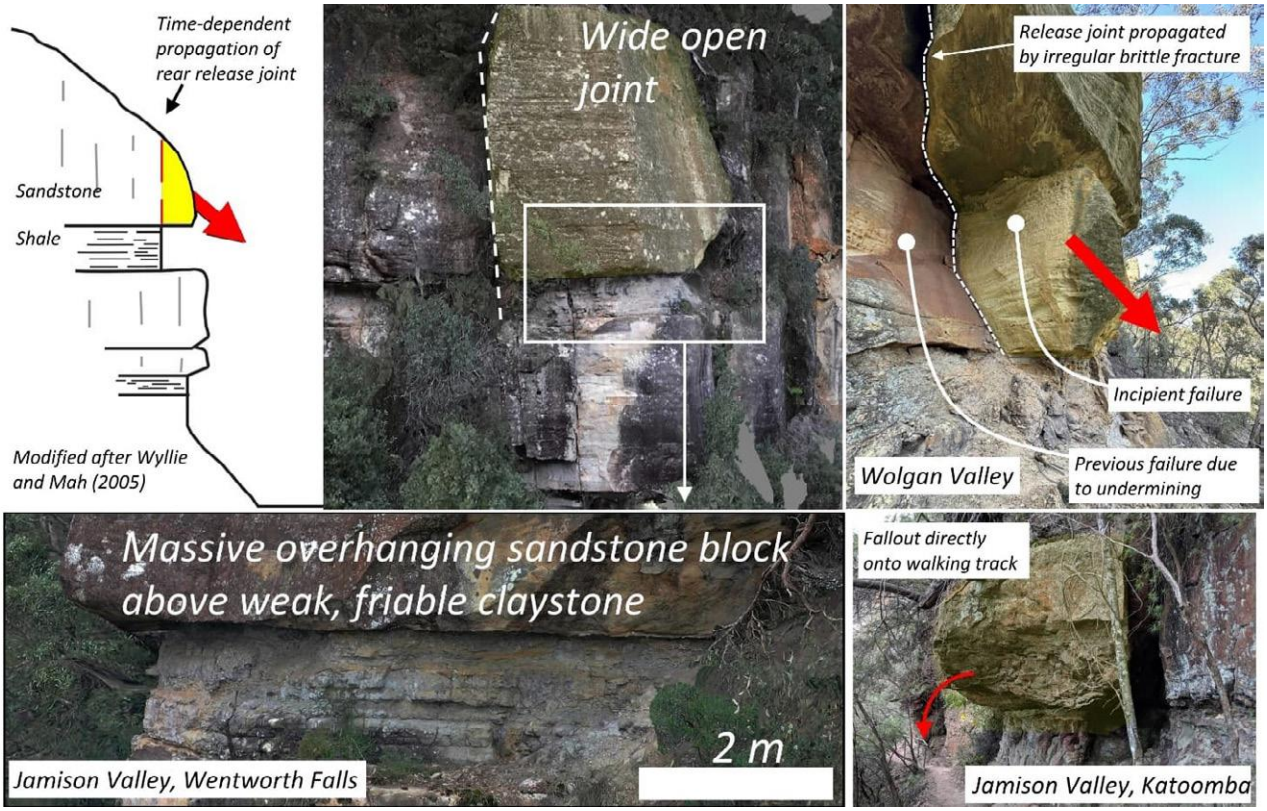

Figure 5: Examples of undermining by erosion of weak shale or claystone

Although the two processes of joint propagation and shale undermining may occur simultaneously, field evidence suggests that vertical rear release joints are often fully developed and significantly dilated many years before failure occurs in the underlying shale. However, if no basal shale layer is present, then failure of a "freestanding" overhang should be controlled by the propagation of rear and lateral release joints. The next section introduces a numerical modelling technique to model the time-dependence of these two failure mechanisms.

4 DISCRETE ELEMENT METHOD METHODOLOGY

4.1 THE BONDED BLOCK METHOD

The bonded block method (BBM) is a subset of the discrete element method where intact material is represented by an assembly of 2D polygons or 3D polyhedra with strong, stiff contacts; breakage of the bonded contacts simulates the process of brittle fracture. Previous BBM research has investigated the use of polygonal Voronoi tessellations to represent brittle failure of strong intact rock and jointed rock masses (Christianson et al., 2006; Alzo'ubi, 2009). Voronoi tessellations produce an assembly of random interlocking polygons that tends to produce a stiff macroscopic response predisposed to localised tensile contact failure with rough, irregular failure surfaces. This study applies the trigon discretisation methodology in *UDEC*, first introduced by Gao (2013), where Voronoi polygons are further subdivided into triangular blocks. In contrast with Voronoi models, trigon discretisation allows a greater degree of kinematic freedom in the bonded block assembly. Whereas the macroscopic response of Voronoi models is strongly influenced by particle interlocking effects, trigon models can be more directly controlled by the strength and stiffness of bonded contacts. Previous research has demonstrated the ability of trigon models to simulate laboratory scale failure of coal measures rocks and field scale failure of underground coal mine roadways (Gao and Stead, 2014). The BBM

trigon technique has also been applied to large rock slope failures mechanisms including flexural toppling (Zheng et al., 2018) and mining-induced collapse of sandstone cliffs in the Blue Mountains (Tuckey, 2023).

A significant advantage of the BBM method is the ability to model non-persistent discontinuities that terminate in intact rock, with the breakage of bonded block contacts simulating fracture propagation. Figure 6 illustrates a conceptual example of a fractured rock slope containing multiple scales of pre-existing discontinuities varying from microcracks through to high persistence joints and faults. A non-daylighting sliding surface is included near the toe of the slope. Conventional discrete element models require convex blocks with complete perimeters; to accommodate computing limitations the model will exclude discontinuities below a lower bound persistence limit, while retaining the key high persistence discontinuities that are expected to control slope kinematics. Bandis (2004) described this in terms of the "effective block" concept, with block properties adopting scaled stiffness and shear strength parameters to account for low persistence and incipient discontinuities that are not explicitly included in the model.

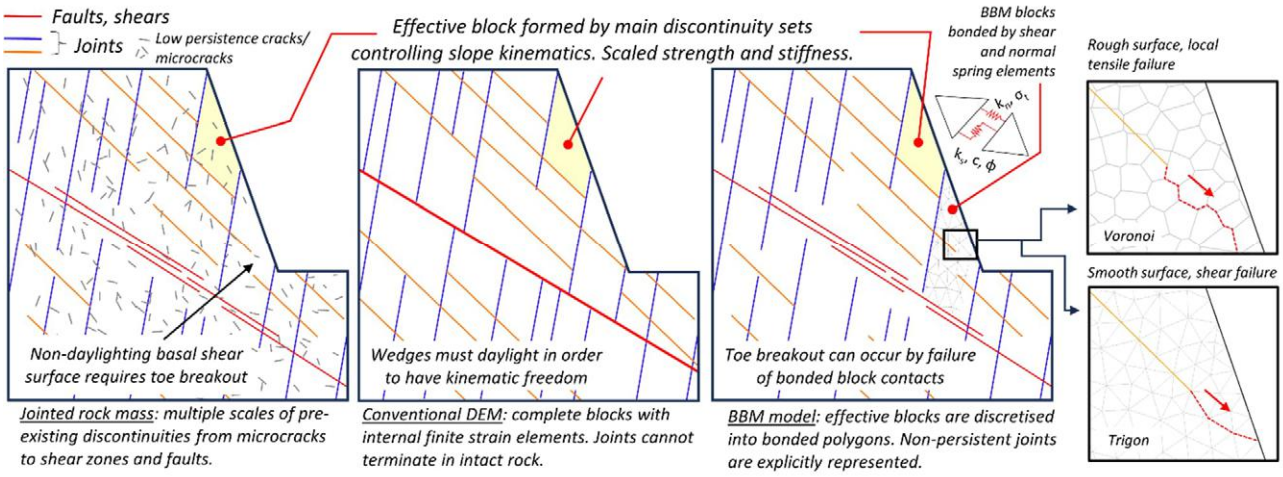

Figure 6: Conceptual illustration of the effective block concept and BBM discretisation

While the conventional discrete element model cannot explicitly include a non-daylighting wedge, the BBM approach can simulate toe breakout along a rough, irregular failure surface that develops by localised contact tensile failure in the case of Voronoi discretisation, or a smooth failure surface dominated by contact shear failure for a trigon model. The next section describes the implementation of a fracture mechanics model in *UDEC* for modelling time-dependent degradation of bonded block contact cohesion and tensile strength, driven by subcritical crack growth.

4.2 A FRACTURE MECHANICS MODEL FOR SUBCRITICAL CRACK GROWTH

Kemeny (2003) introduced a fracture mechanics model to simulate the effect of intact rock bridges along a planar sliding surface subject to constant normal stress. Time-dependent reduction in cohesion was calculated using a closed-form solution for subcritical crack growth assuming a mode II (shear) failure mechanism. Kemeny (2005) extended the approach using the discrete element method software *UDEC* to simulate time-dependent cohesion loss in pre-existing joints surrounding an underground excavation, accounting for changing stress conditions as the zone of damage (i.e. excavation-induced fractures) develops around the tunnel profile. Sampaleanu (2017) further developed the model, incorporating mode I (tensile) failure of bonded Voronoi blocks into analysis of rockfall in an open pit mine slope.

The subcritical crack growth model is based on an idealised coplanar or "in plane" rock bridge of width $2a$ separating the tips of two pre-existing discontinuities in a rock block of width of $2w$. Failure can occur in mode I (tension) or mode II (shear). It is assumed that failure will occur when the mode I stress intensity K_I or mode II stress intensity K_{II} exceeds the fracture toughness parameters K_{IC} or K_{IIC} which are material properties of intact rock with units of $MPa\sqrt{m}$. By considering the limit state where $K_{II} = K_{IIC}$ the equation for mode II stress intensity can be re-arranged to estimate the initial cohesion of a bonded contact c_0 as a function of rock bridge geometry and fracture toughness:

$$Rock\ bridge\ cohesion = c_0 = \frac{K_{IIC}\sqrt{\pi a}}{2w} \quad (1)$$

Equation 2 shows the corresponding equation for initial rock bridge tensile strength σ_{t0} as proposed by Sampaleanu (2017), considering mode I (tensile) failure occurring when $K_I = K_{IC}$.

$$Rock\ bridge\ tensile\ strength = \sigma_{t0} = \frac{K_{IC}\sqrt{\pi a}}{2w} \quad (2)$$

Figure 7 illustrates the conceptual rock bridge model under mode I (tensile) and mode II (shear) loading conditions. The stress intensity factors depend on the specimen width *2w*, the rock bridge half width *a*, and the imposed loads. Mode I stress intensity K_I is calculated using the normal stress σ_n and mode II stress intensity K_{II} is calculated using mobilised cohesion ($\tau - \sigma_n \tan \varphi$) where τ is shear stress and φ is the friction angle of the two pre-existing discontinuity segments. At the limit state these equations can be rearranged to estimate the initial cohesion and tensile strength provided by the intact rock bridge. Conversely, if the initial joint cohesion, tensile strength and fracture toughness is known, then the same equations can be re-arranged to calculate the initial rock bridge width *2a*.

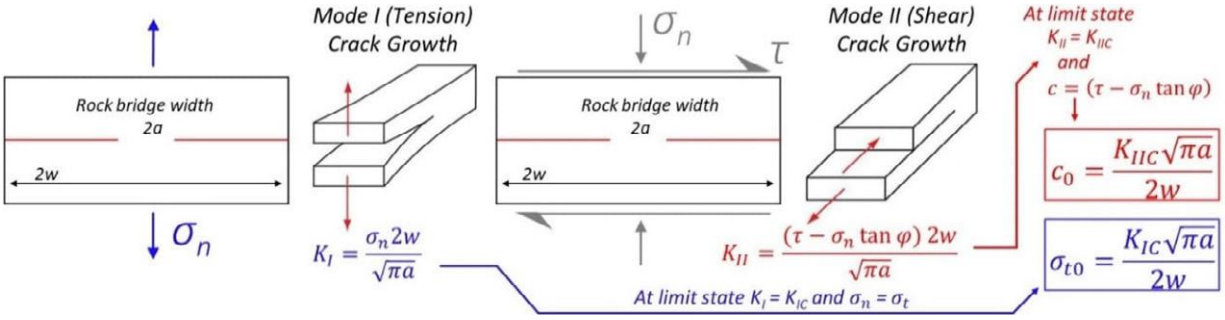

Figure 7: Rock bridge model with formulae for stress intensity used to estimate cohesion and tensile strength

After the initial BBM tensile strength and cohesion are defined, a strength degradation algorithm is applied at each numerical timestep. Over time, subcritical crack growth causes the rock bridge width *2a* to decrease, reducing the cohesion and tensile strength provided by the rock bridge. Kemeny (2005) proposed that the rate of subcritical crack growth could be estimated using a version of the Charles power law adapted for mode II loading, where crack growth velocity is calculated using the ratio of mode II stress intensity K_{II} to the critical mode II fracture toughness parameter K_{IIC} and material constants *A* and *n* which are properties of intact rock that can be measured in the laboratory:

$$Subcritical\ shear\ crack\ growth\ velocity = a'(t) = A\left(\frac{K_{II}}{K_{IIC}}\right)^n \tag{3}$$

For this investigation, the Charles law equation is modified to consider the combined effects of mode I and mode II crack growth. The local magnitudes of K_I and K_{II} for each bonded contact are used to resolve an effective stress intensity K_{EFF} which is compared against a weighted fracture toughness parameter that accounts for the relative proportions of mode I and mode II loading. After calculating the subcritical crack growth velocity for each contact, it is necessary to estimate a suitable timestep Δt so that the change in rock bridge width can be calculated as follows:

$$Change\ in\ rock\ bridge\ width = \Delta a = a'(t) \times \Delta t \tag{4}$$

UDEC applies an explicit finite difference solution scheme to solve the equations of force and motion for block contacts and internal finite strain elements within deformable blocks, based on a mechanical timestep that is not directly relatable to real time. This study therefore assigns a "subcritical timestep" Δt at each calculation cycle, such that an upper bound subcritical timestep in the order of 10^7 seconds is adopted for low stress conditions; this limit has been demonstrated to produce stable results for modelling of long-term strength reduction over hundreds to tens of thousands of years (Kemeny, 2005). The subcritical timestep decreases exponentially to a minimum of 10 seconds as stress intensity approaches the limiting fracture toughness. After calculating the reduction in rock bridge width, equation 1 is used to calculate the updated (reduced) contact cohesion; the reduction in contact tensile strength is assumed to be proportional to the reduction in contact cohesion. Cycling is then continued until failure is observed.

In summary, the strength degradation algorithm applies the following steps, looping through all bonded block contacts at every mechanical timestep:

- **Step 1:** Read current values for cohesion *c*, friction angle φ, current tensile strength σ_t. Calculate the current rock bridge length a_0 for each contact, based on the current contact cohesion, by re-arranging the equation for mode II stress intensity as shown below:

$$Current\ rock\ bridge\ length\ = a_0 = \left(\frac{c\ 2w}{K_{IIC}\sqrt{\pi}}\right)^2 \tag{5}$$

- **Step 2:** Read contact shear force, normal force, and contact length. Shear and normal stresses are derived by dividing forces by contact length. Calculate stress intensity parameters K_I and K_{II} for each bonded contact.
    - Calculate the effective stress intensity for each contact, accounting for mode I and mode II loading:

$$K_{EFF} = \sqrt{K_I^2 + K_{II}^2} \tag{6}$$

- Find the maximum stress intensity $K_{EFF(MAX)}$ occurring in the model and calculate an appropriate subcritical timestep Δt such that the maximum timestep is in the order of 10^7 seconds. For the given model conditions, the following equation was adopted:

$$\Delta t = (1.33 \times 10^8) \times e^{(-3.28\times10^{-5})\times K_{EFF(MAX)}} \quad (7)$$

- Crack growth rate $a'(t)$ is calculated for each bonded contact, using a modified version of Equation 3 that incorporates both mode I and mode II stress intensity:

$$Subcritical\ crack\ growth\ velocity = a'(t) = A\left(\frac{K_{EFF}}{\frac{2\theta}{\pi}K_{IC}+(1-\frac{2\theta}{\pi})K_{IIC}}\right)^n = A\left(\frac{K_{EFF}}{K_{C(EFF)}}\right)^n \quad (8)$$

$$\text{Where } \theta = tan^{-1}\frac{K_I}{K_{II}}$$

- Use the crack growth rate $a'(t)$ and subcritical timestep Δt to calculate the new rock bridge width:

$$a_1 = a_0 + (a'(t) \times \Delta t) \quad (9)$$

- **Step 3**: Use the new rock bridge width a_1 to calculate the updated value of cohesion according to equation 1. The reduction in contact tensile strength is assumed to be proportional to the reduction in contact cohesion. New cohesion and tensile strength values are assigned to the bonded contact. Cycling is continued until failure is observed. The rate of tensile and shear contact failure versus accumulated subcritical time is recorded.

Figure 8 shows a graphical representation of the strength degradation algorithm; note that the edges of each bonded trigon element are each discretised into two bonded half-lengths of dimension $2w$.

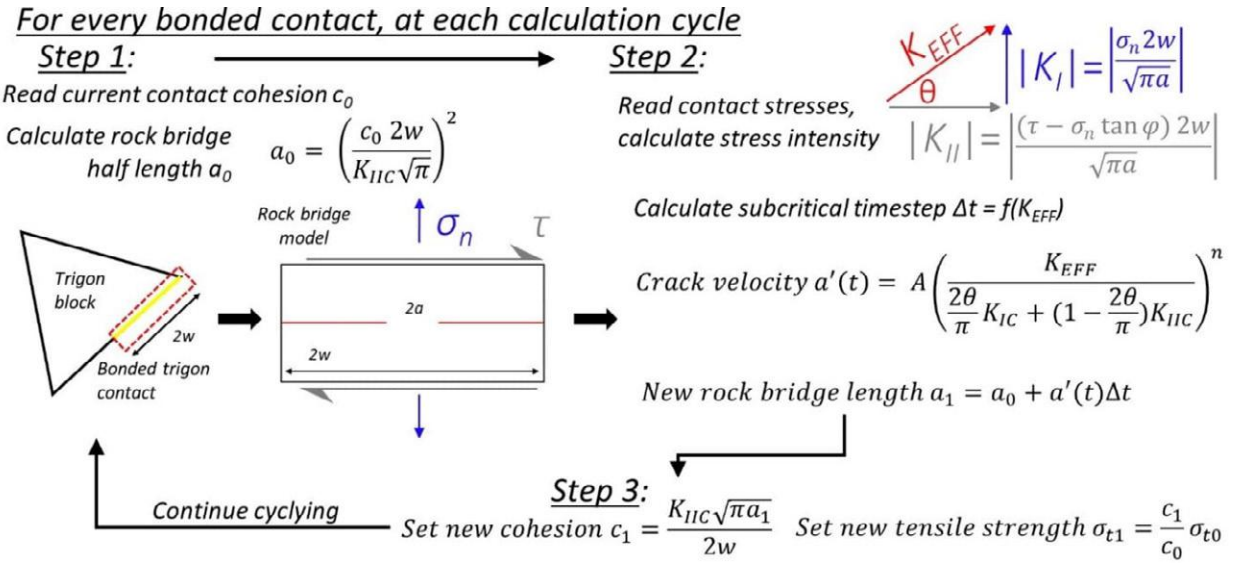

Figure 8: Strength degradation algorithm carried out at each mechanical timestep for every BBM contact

Section 5 presents a conceptual numerical modelling study of an overhanging sandstone slab, where the BBM strength degradation algorithm is used to simulate time-dependent loss of bonded contact cohesion and tensile strength, leading to failure by propagation of a non-persistent vertical release joint. Section 6 extends the modelling technique to consider time-dependent rockfall initiation by preferential undermining failure of a weak shale or claystone layer.

5 TIME-DEPENDENT FAILURE OF AN OUTCROP-SCALE OVERHANG

5.1 MODEL SETUP

A simplified outcrop-scale model was constructed to consider an overhanging slab of massive sandstone. Failure occurs by propagation of a non-persistent vertical rear release joint. The overhanging slab is 5 m high and 1 m wide. Various intact rock bridge geometries were modelled, with the bridge placed at the top, middle, or bottom of the slab, and a further scenario with intact rock bridges distributed across the joint. The distributed rock bridge scenario represents the pre-existing joint as fully persistent contact interrupted by strong rock bridge segments of 0.25 m length; the other scenarios model the joint as a non-persistent discontinuity with explicit terminations in intact rock. Figure 9 shows the model geometry, with a region of 0.2 m edge length trigon blocks bonded to a far field elastic continuum.

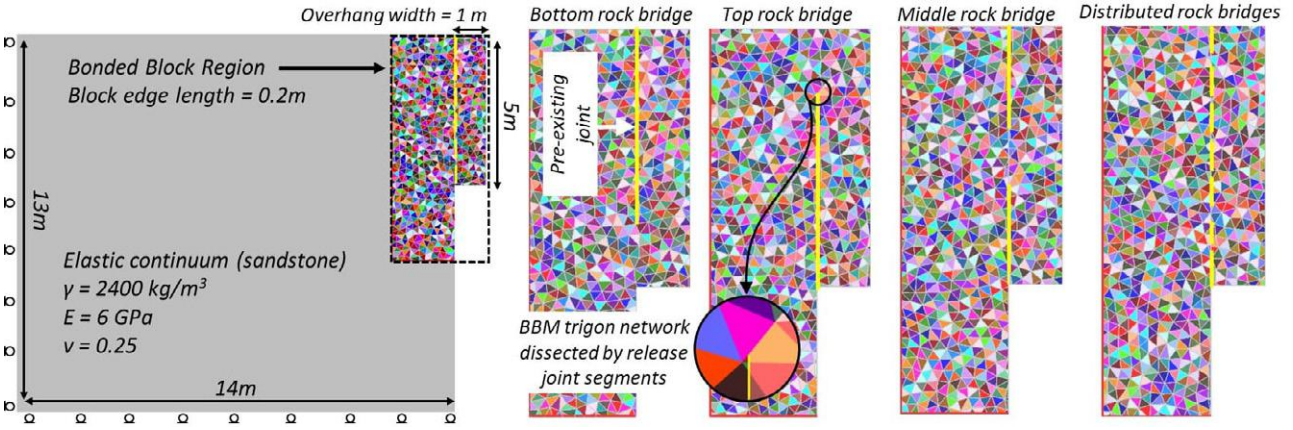

Figure 9: Geometry of simple overhang stability model with variable rock bridge geometry

The pre-existing vertical joint is modelled as a frictional surface with zero cohesion and tensile strength. In situ stresses are initialised according to gravitational self-weight and displacement versus time is recorded at the crest of the cliff. Intact rock bridge content is varied from 5% to 30% representing a total intact rock bridge length of 0.25 m to 1.5 m measured vertically from the non-persistent joint tips. BBM contact parameters are derived from laboratory-scale trigon simulations by Tuckey (2023) to represent good quality Class I/II sandstone under the Sydney Rock Mass Classification System as described by Bertuzzi and Pells (2002) and Oliveira (2014). Table 1 summarises material parameters used to define the strength and stiffness of bonded blocks and the pre-existing joint. Stiffness parameters for BBM contacts are scaled according to the recommendations of Itasca and Christianson et al. (2006) as a function of BBM contact length. The initial BBM cohesion and tensile strength consider a bonded trigon contact half-length $2w$ of 0.1 m comprised of 50% initial rock bridge ($2a$ = 0.05 m). Fracture toughness parameters K_{IC} and K_{IIC} are estimated from intact rock brittleness indices that depend on UCS and tensile strength σ_t after Nejati and Moosavi (2017).

Table 1: Summary of key input parameters to simple overhang model

Application	Parameter	Sandstone	Pre-existing joint
Intact Rock	Density ρ (kg/m^3)	2400	n/a
	Reference UCS σ_c (MPa)	25	
	Reference Tensile Strength σ_t (MPa)	2.5	
	Young's Modulus E (GPa)	6	
Bonded trigon block contacts	Mode I Fracture Toughness K_{IC} (MPa $\sqrt{\text{m}}$)	0.4	
	Mode II Fracture Toughness K_{IIC} (MPa $\sqrt{\text{m}}$)	0.8	
	Initial contact cohesion c_0 (MPa)	2.2	0
	Initial contact tensile strength σ_{t0} (MPa)	1.1	0
	Contact Friction angle φ	35°	36°
	Contact normal stiffness j_{kn} (GPa/m)	360	10
	Contact shear stiffness j_{ks} (GPa/m)	144	1
	Subcritical parameter A (m/s)	0.2	n/a
	Subcritical parameter n	16	

Subcritical crack growth parameters A and n are based values published by Lee (2007) who modelled time-dependent failure of slopes in Coconino sandstone, and Ko and Kemeny (2011) who undertook laboratory investigations of subcritical crack growth in Coconino sandstone from Arizona, USA, using a variety of test techniques including the double torsion test, wedge splitting test, double cantilevered beam test, and modified punch-through shear test.

At laboratory scale the crack velocity parameter A can vary across several orders of magnitude from 10^{-4} to 10^{-1} m/s. The parameters adopted for this investigation are upper bound estimates, which are considered suitable for these field-scale simulations. The upper bound crack growth velocity estimates implicitly account for exogenous environmental factors that may accelerate crack growth, but are not directly included in the model, such as: root jacking from trees growing into pre-existing discontinuities; thermally induced strains based on daily and seasonal temperature fluctuations; and water infiltration into joints from surface water runoff and groundwater seepage.

5.2 RESULTS

The results demonstrate that the brittle failure mechanism and subcritical time required for failure to develop vary significantly depending on the geometry and proportion of intact rock bridges. When the intact rock bridge is positioned at the base of the slab, failure involves progressive development of an irregular tensile fracture surface that propagates downward from the bottom tip of the pre-existing joint, initially curving back from the free face. Figure 10 shows the contours of block displacement, failed contact states, and stress intensity for BBM contacts at timesteps from 916 years up to failure (kinematic release) after 2640 years of simulated "subcritical time".

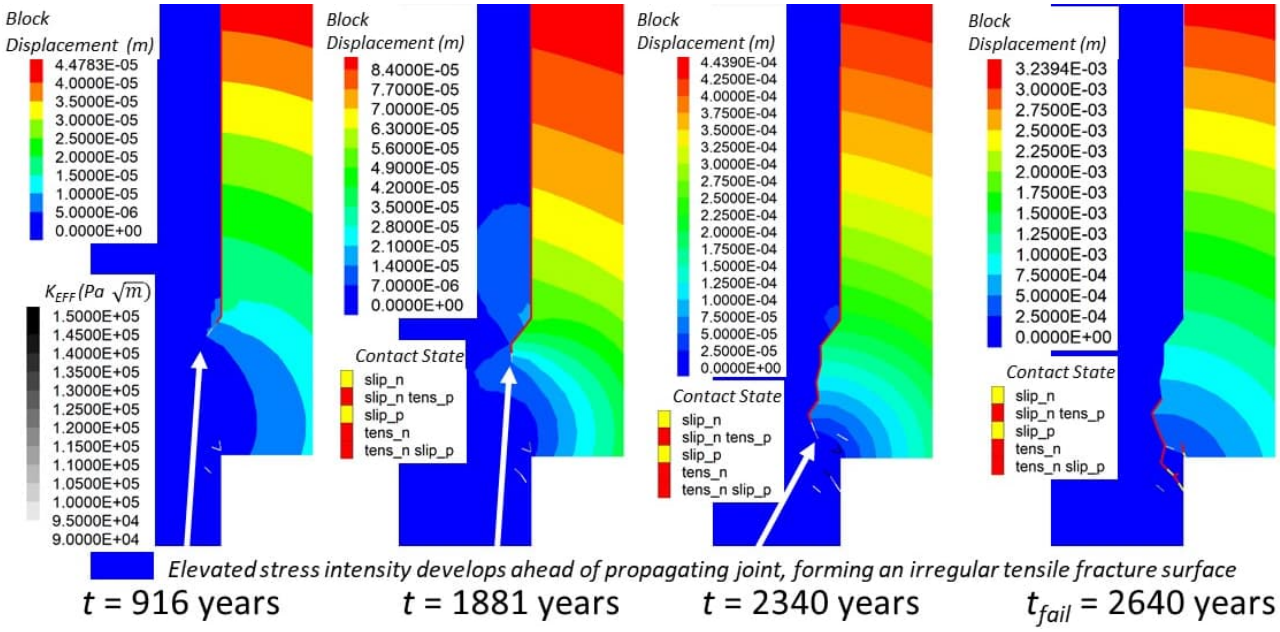

Figure 10: Examples results for a 1.5m (30%) bottom rock bridge failing after 2640 years

The history plots of maximum stress intensity $K_{EFF(MAX)}$ and subcritical timestep Δt shows how the crack growth simulation "slows down" as stress intensity increases ahead of the advancing crack front (Figure 11). The right-hand plot shows the history of crack length (BBM contact length failed in tension and shear), and cliff crest displacement.

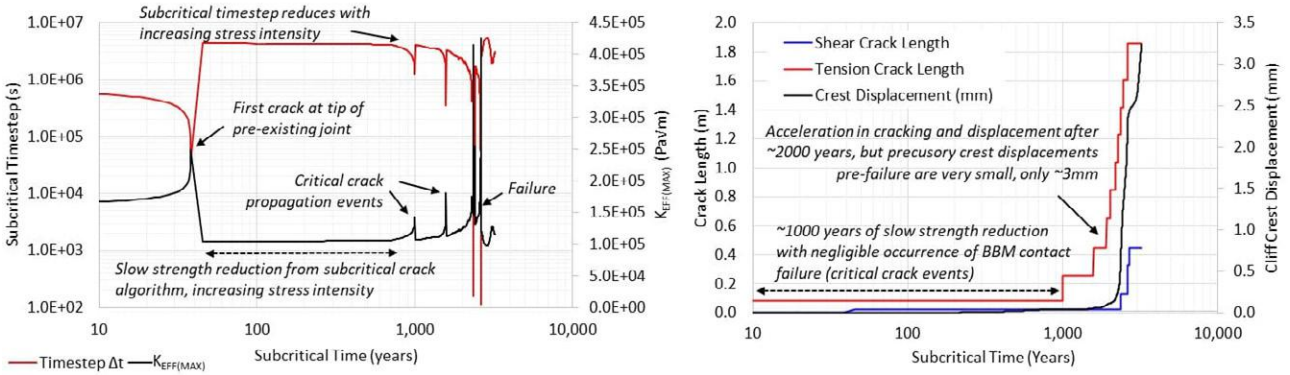

Figure 11: Histories of $K_{EFF(MAX)}$, subcritical timestep, displacement, and crack length (1.5m bottom rock bridge)

Subcritical crack growth is modelled as a continuously active process, simulated by the progressive reduction in BBM cohesion and tensile strength. In contrast, the failure of BBM contacts in shear or tension represent episodic processes involving critical crack growth events with rapid failure of bonded contacts. For the model incorporating a "bottom rock bridge" at the base of the rockfall slab, subcritical crack growth dominates during the first 1000 years of simulation time, with episodic critical crack growth events occurring between 1000 and 2600 years, leading up to failure. Precursory displacements at the crest of the slab are limited to about 3 mm. Tensile cracks dominate the failure process.

The failure mechanism and "subcritical time" required for failure to develop vary depending on the rock bridge content and geometry. Figure 12 illustrates the failure mechanisms that develop for the maximum rock bridge scenario, with approximately 30% of the rear release surface comprising intact rock bridges placed either at the top of the slab, in the

middle of the rear release joint, or distributed across the rear release surface. The plots of total BBM crack length versus subcritical time shows how the subcritical time required for failure to develop may vary from hundreds of years for the "top rock bridge" geometry, to tens of thousands of years for the "distributed rock bridge" geometry. For the top, middle, and distributed rock bridge scenarios, failure develops in a "bottom-up" process, with release of a lower "sub-slab" by propagation of subhorizontal tensile fractures. The time to failure appears to depend on the height of this critical "sub-slab" which is determined by rock bridge geometry. The "top rock bridge" scenario imposes the highest tensile loading because this geometry produces the greatest effective "sub-slab" slab height.

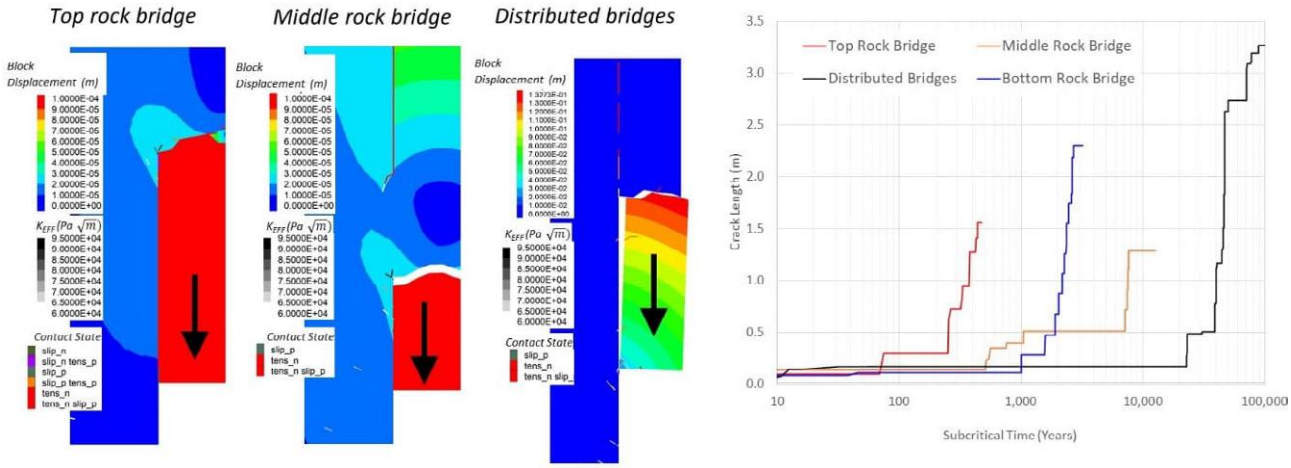

Figure 12: Comparison of failure mechanisms for top, middle, and distributed rock bridges (30% length)

Figure 13 shows the corresponding results for the 10% rock bridge scenario. The time to failure is reduced by roughly two orders of magnitude when compared with the 30% rock bridge case. Failure develops fastest for the bottom rock bridge scenario, after approximately 10 years, with two discrete shear cracking events in the basal rock bridge. Tensile failure occurs after approximately 100 years for the "top rock bridge" scenario. The "middle rock bridge" failure involves release of a basal slab after 330 years, and release of the remaining upper slab after about 800 years.

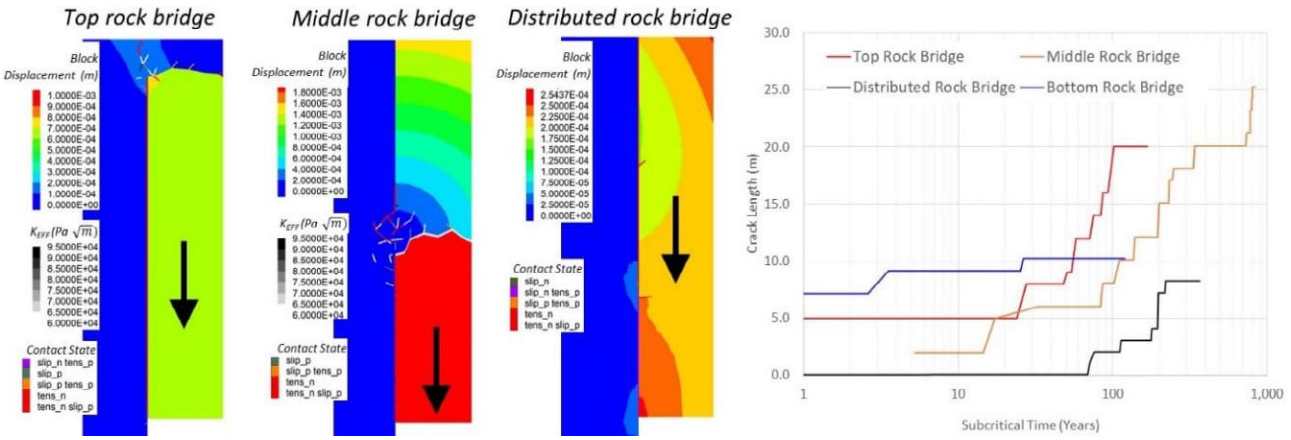

Figure 13: Comparison of failure mechanisms for top, middle, and distributed rock bridges (10% length)

The results demonstrate how the rock bridge geometry influences the brittle failure mechanism and timespan required for failure. Larger intact rock bridges require more time for interaction to develop between the tips of pre-existing joints, and the brittle release surface tends to propagate sub-horizontally. As the rock bridge length is decreased, incipient brittle fractures interact earlier, forming a composite release surface sub-parallel to the rear release joint.

Figure 14 presents a semi-logarithmic plot of time to failure t_f versus rock bridge content for each case. A secondary horizontal axis indicates the corresponding persistence of the rear release joint, with an inferred "zero" point included where time to failure t_f is assumed to be less than 0.1 years for 0% rock bridges, representing effectively instantaneous failure in the case of a fully persistent rear release joint. The 25% and 30% "distributed rock bridge" scenarios apply an accelerated subcritical timestep to achieve manageable computation times, due to the reduced stress intensity that occurs when the weight of the overhanging slab is distributed across a greater number of intact rock bridges.

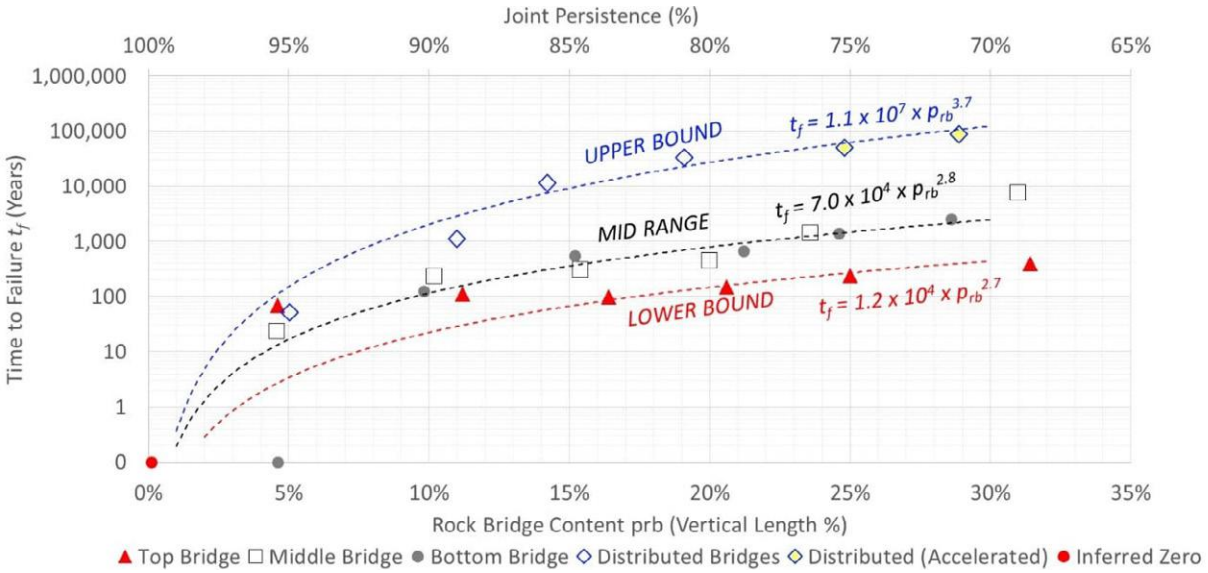

Figure 14: Time to failure versus rock bridge content for various rock bridge geometry scenarios

Power law curves appear to give a reasonable conceptual fit to upper bound and lower bound trends for time to failure t_f versus rock bridge content. Key observations include:

- The distributed rock bridge geometry scenarios produce the longest time to failure t_f because subcritical crack growth rate is proportional to stress intensity, and when the weight of the slab is distributed among a greater number of rock bridges, the stress intensity at any one rock bridge is reduced.
- The top rock bridge geometry produces the most rapid failures; this is interpreted to occur because these scenarios subject the rock bridge to direct tension loading and the greatest effective "sub-slab" height.
- When rock bridge content is reduced below 5% to 10% there is a marked decrease in stability, with time to failure decreasing by roughly an order of magnitude for every 3% decrease in rock bridge content.

The results reflect the dependence of the subcritical crack growth rate on localised stress concentrations at the tips of pre-existing joints. The next section extends the time-dependent strength degradation model to consider failure of a sandstone cliff by progressive undermining of a weaker underlying shale layer.

6 PROGRESSIVE CLIFF-SCALE COLLAPSE PROMOTED BY UNDERMINING

6.1 MODEL SETUP

The subcritical crack growth model introduced in the previous section was extended to consider time-dependent brittle failure of an overhanging sandstone cliff undermined by a layer of weaker shale or claystone, representing a common landform in Blue Mountains National Park. Figure 15 shows the model geometry, incorporating a 50 m high cliff, with the upper 20 m forming an overhanging sandstone face underlain by a 4 m thick layer of weaker shale. The shale and upper sandstone rock masses are discretised into trigon elements of 0.6 m length, bonded to a far-field elastic continuum. The lower half of the cliff is represented by jointed elastic sandstone blocks. The trigon discretisation is overprinted by pre-existing joints and bedding discontinuities with negligible cohesion and tensile strength.

Discontinuity geometry and rock block shapes reflect observations from geotechnical mapping of sandstone cliffs in the Blue Mountains (e.g. Tuckey, 2023). Discontinuity spacing is "upscaled" and bonded trigon block edge lengths are limited to 0.6 m to manage computational requirements, while retaining key structural controls slope failure kinematics. The reference properties for sandstone are unchanged from the previous outcrop-scale models.

The shale layer is based on a Class II shale with intact rock UCS of 15 MPa, with calibrated BBM contact parameters derived from Tuckey (2023). The reference fracture toughness values are K_{IC} = 0.25 MPa $\sqrt{m}$ in tension and K_{IIC} = 0.6 MPa $\sqrt{m}$ in shear, based on relationships with UCS and σ_t as proposed by Nejati and Moosavi (2017). Initial BBM cohesion and tensile strength are calculated using the same initial rock bridge geometry as the outcrop-scale model, where $2w$ = 0.1 m and $2a$ = 50 mm. The subcritical timestep Δt is calculated from the maximum stress intensity ratio $K_{EFF}/K_{C(EFF)}$ such that the maximum subcritical timestep is in the order of 10^7 seconds or less, reducing exponentially as stress intensity increases to maintain numerical stability.

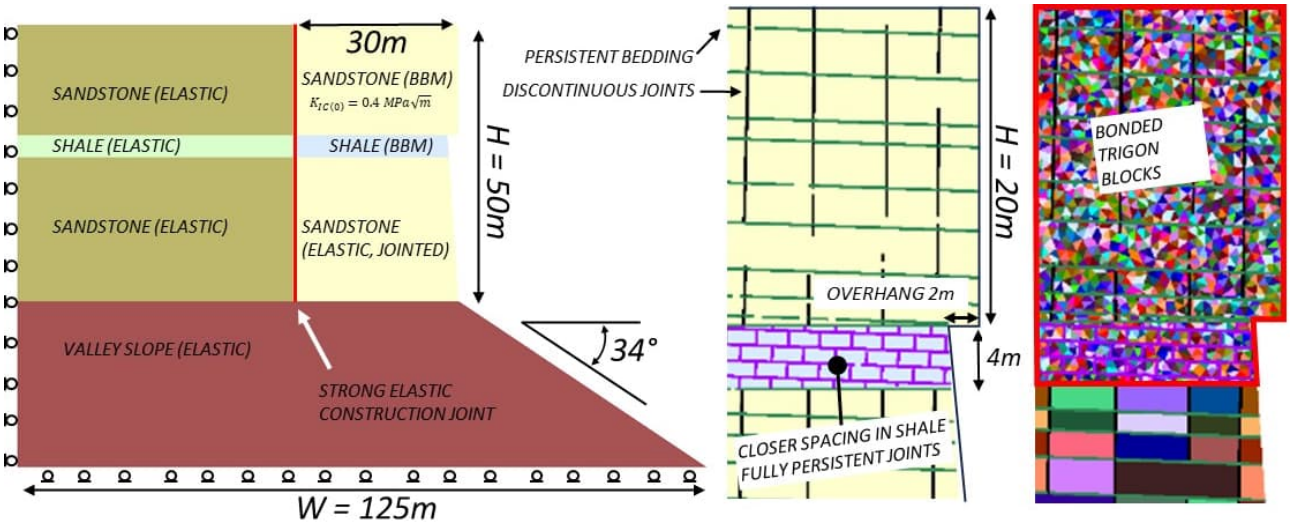

Figure 15: Geometry of cliff scale model with bonded block region surrounding a sandstone overhang

While the outcrop-scale model in the previous situation adopted uniform values for bonded contact strength and subcritical crack growth parameters A and n, the cliff scale model incorporates additional calculations to account for the influence of confining stress in suppressing subcritical crack growth. Laboratory experiments have measured how confining stress suppresses crack growth and increases the critical fracture toughness parameters K_{IC} and K_{IIC} while also reducing subcritical crack growth velocity. Changes to fracture toughness and the subcritical crack growth parameter n can be simplified as a linear, whereas the subcritical A parameter decreases exponentially with increasing confinement. Figure 16 shows the relationships adopted for the cliff-scale model, based on published values for sandstone from Backers (2004), Lee (2007), and Ko and Kemeny (2011). The confinement-dependent parameters yield lower fracture toughness and increased crack velocity where confining stress is low: consequently, the model should demonstrate how brittle failure fist develops in the unconfined near-surface rock mass at the cliff face.

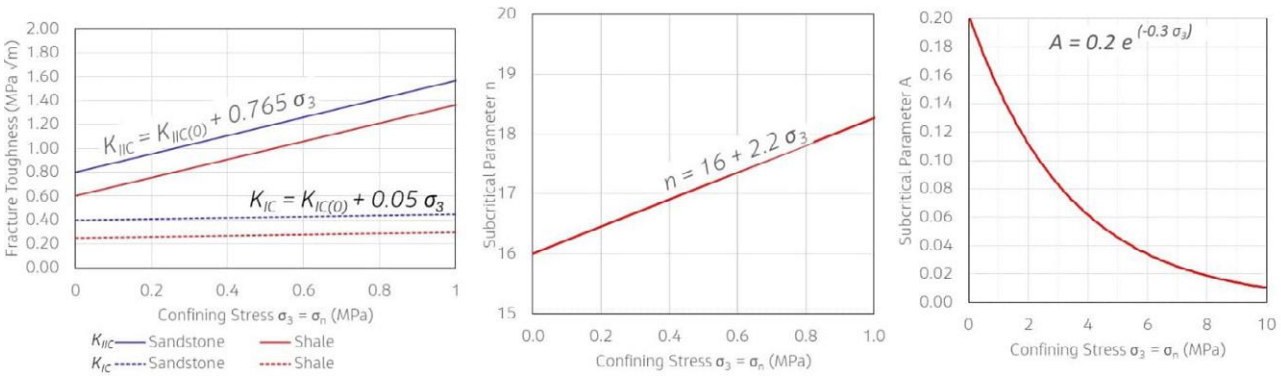

Figure 16: Fracture toughness and subcritical crack parameters versus confining stress

Two different *in situ* stress scenarios were investigated: the first scenario considers a lithostatic stress regime, assuming that high horizontal tectonic stresses have been relieved by slow, long-term escarpment retreat and erosion. The second scenario applies a high horizontal major principal stress ($\sigma_1 = \sigma_x = \sigma_H$) based on the relationships proposed by Oliveira and Parker (2014), who demonstrated the dependence of *in situ* stress on rock mass stiffness in the layered sedimentary formations of the Sydney Basin, where the sandstone units are stiffer and thus attract higher horizontal stresses than the softer shale units. Both scenarios adopt the following modelling sequence:

- **Step 1:** Initialise *in situ* stresses for a rectangular model domain representing the subsurface profile before any valley incision has occurred. Vertical stress $\sigma_y = \sigma_v$ is calculated using an average unit weight for the rock mass of 23.5 kN/m^3. The lithostatic scenario then sets horizontal stress $\sigma_x = \sigma_H$ equal to vertical stress. The high horizontal stress scenario adopts horizontal stresses as summarised below:

$$\textbf{\textit{Sandstone}}\ \sigma_x = \sigma_H = 3\ \sigma_V + 1\ \text{MPa} \tag{10}$$

$$\textbf{\textit{Shale}}\ \sigma_x = \sigma_H = 1.4\ \sigma_V + 0.4\ \text{MPa} \tag{11}$$

- **Step 2:** Excavate the valley. Cycle the model until equilibrium is reached, using artificially strong BBM contact properties to prevent failure due to rapid stress changes associated with the instantaneous removal of confinement. Stresses redistribute to accommodate the escarpment morphology and geological structure.
- **Step 3**: Calculate stress-dependent fracture toughness and subcritical crack growth parameters. Use the fracture toughness parameters to derive initial values for BBM cohesion c_0 and tensile strength σ_{t0} considering an initial rock bridge geometry where $2w = 0.1$ m and $2a = 50$ mm as per the outcrop-scale simulations.
- **Step 4:** Activate the shear strength degradation algorithm and cycle the model until failure is observed. The crack growth rate is recorded in terms of the length of BBM contacts failed in tension and shear versus subcritical time. When rock blocks are kinematically freed from cliff face by new brittle fractures, the strength degradation algorithm is temporarily paused, and mechanical cycling is continued to allow the newly detached blocks to fall away from the cliff. Detached blocks are then deleted from the model, and strength degradation algorithm is re-activated to continue modelling long-term subcritical crack growth.

Figure 17 illustrates the influence of *in situ* stress on the confinement-dependent BBM contact strength in terms of the initial cohesion c_0. The lowest BBM cohesion tends to occur on subvertical contacts near the face of the cliff, where confining stress is lowest. With increasing depth behind the cliff face, confining stress and initial BBM cohesion (and tensile strength) increase. The high stress scenario imposes greater confining stress that produces a corresponding increase in the initial BBM cohesion and tensile strength for deeper zones of rock mass, further from the cliff face.

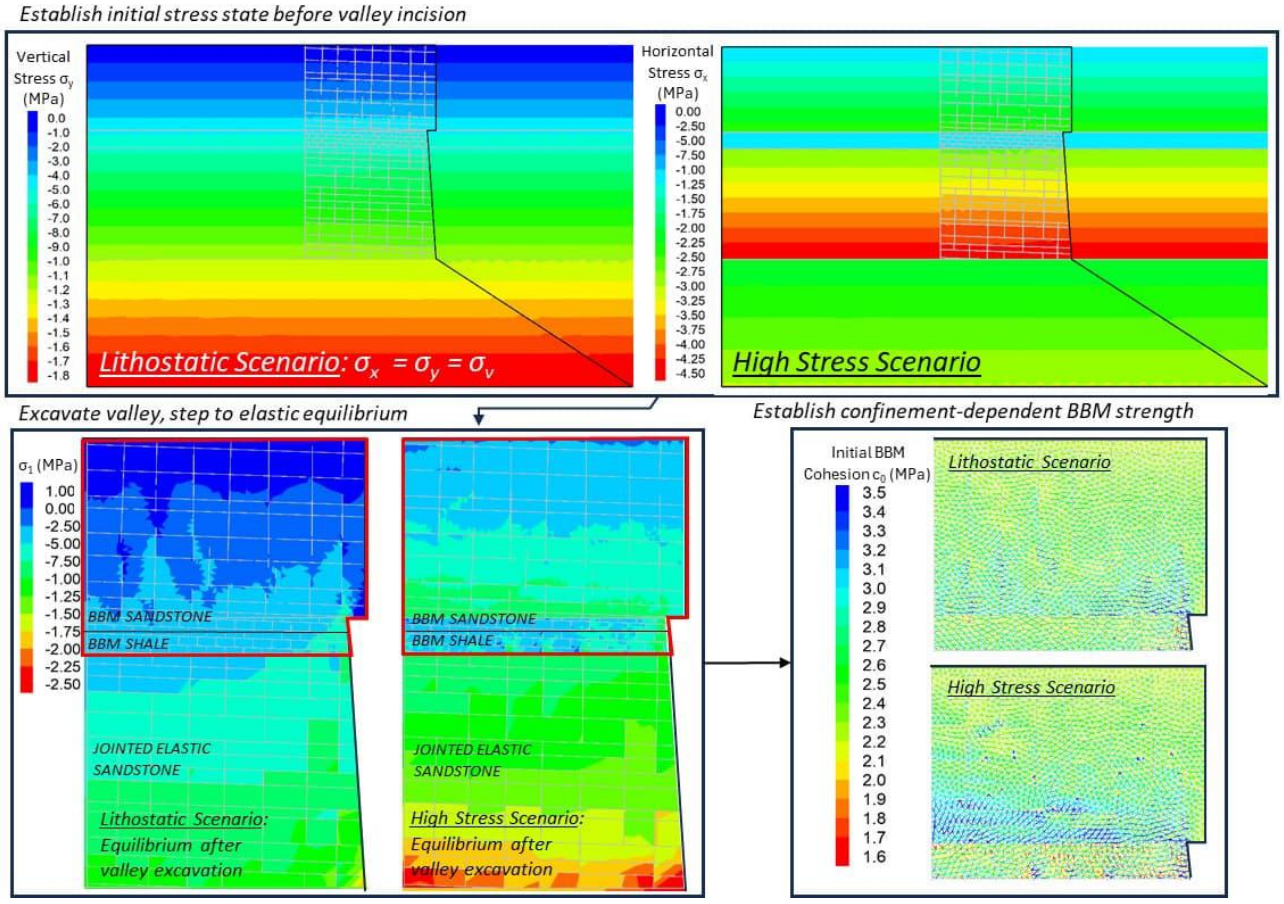

Figure 17: Comparison of stress initialisation and initial BBM strength for lithostatic and high stress scenarios

Although the high stress scenario provides greater confinement and initial BBM strength, it also produces zones of locally elevated normal and shear stress which may act as preferred zones for fracture initiation.

Figure 18 shows the relative change imposed by the high stress scenario, with BBM contacts coloured by the difference in shear stress as fraction of BBM cohesion (ratio τ / c_0) and the difference in tensile normal stresses as fraction of tensile strength (ratio σ_n / σ_{t0}). The accompanying histograms illustrate how the high stress scenario produces a marked increase in shear loading of the BBM shale relative to initial cohesion c_0; increases in tensile loading also occur but are limited to a small number of localised BBM contacts.

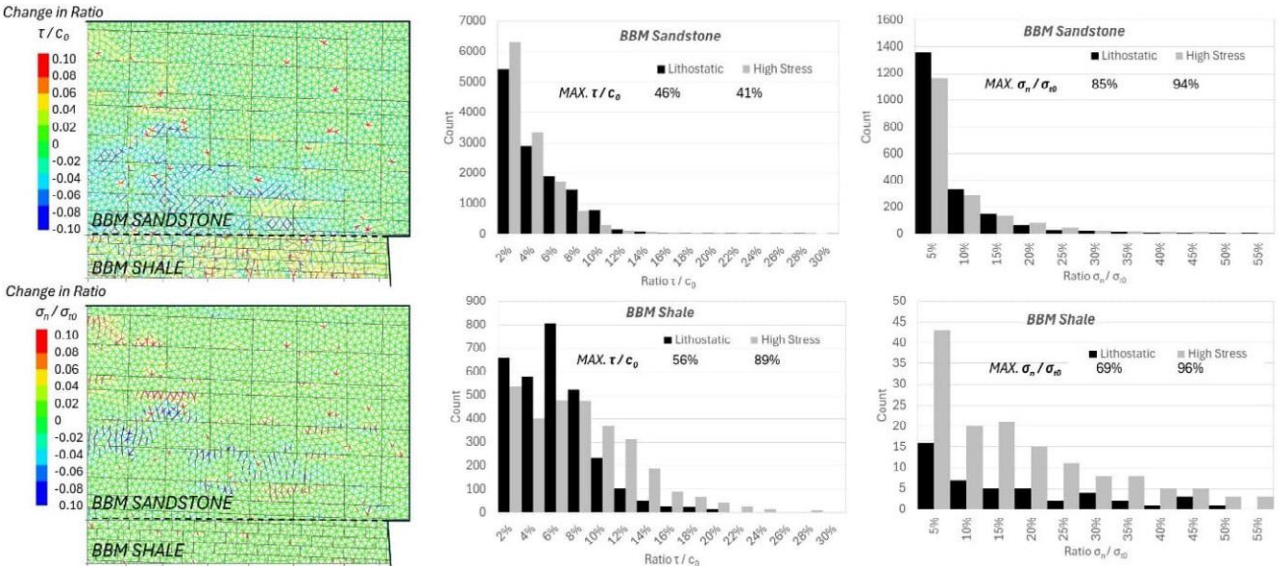

Figure 18: Change in initial stress ratios τ/c_0 and σ_n/σ_{t0} produced by the high stress scenario

The next section shows key results from both *in situ* stress scenarios, focussing on how the initial stress regime influences the rate of subcritical crack growth and the development of time-dependent brittle slope failure.

6.2 RESULTS

Figure 19 shows results from the lithostatic stress model at selected subcritical timesteps from 7.9 years up to 2410 years, focused on BBM discretisation region. Blocks are shaded by rotation in radians to highlight the progressive release of overhanging blocks by new brittle fractures.

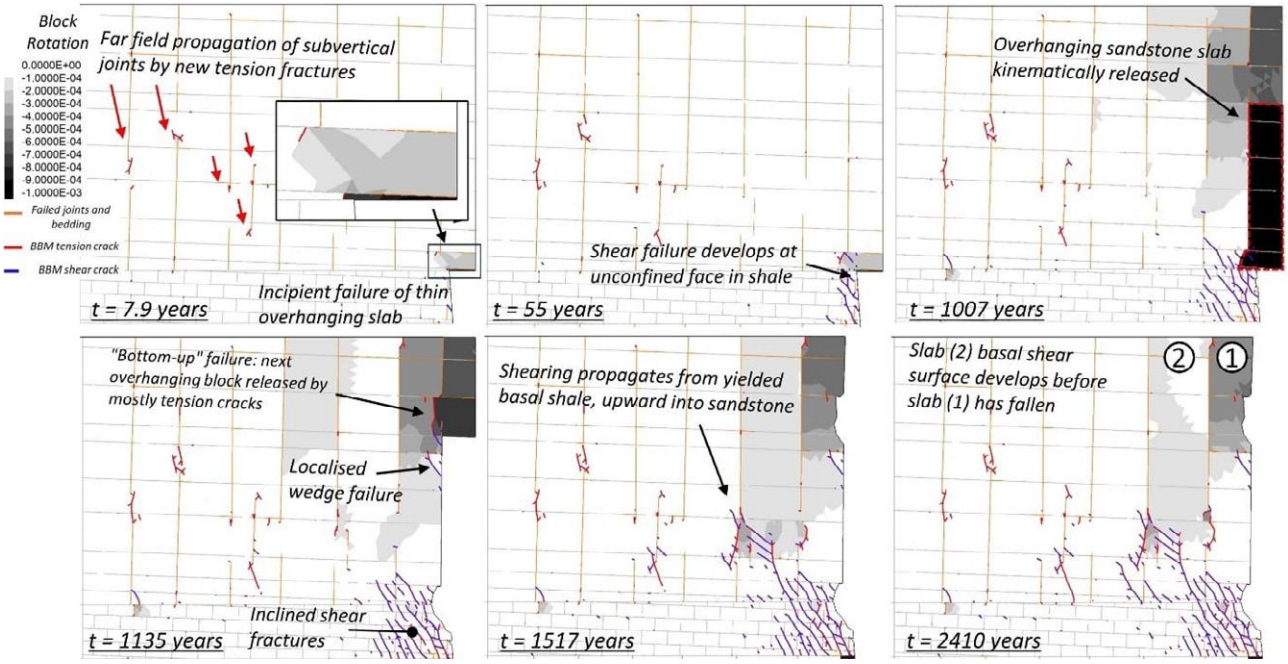

Figure 19: Progressive cliff failure for lithostatic stress scenario

The earliest BBM contact failures involve far-field tension cracking initiating from the tips of non-persistent subvertical joints; this effect demonstrates how the stress field associated with the escarpment landform promotes the propagation of very high persistence vertical joints; this is consistent with field observations of the two regionally ubiquitous, very high persistence orthogonal joint sets that play a critical role in the escarpment retreat processes that produced the modern landscape of the Blue Mountains (Hatherly and Brown, 2022). Figure 20 shows corresponding plots of the high stress scenario for subcritical timesteps up to 1803 years.

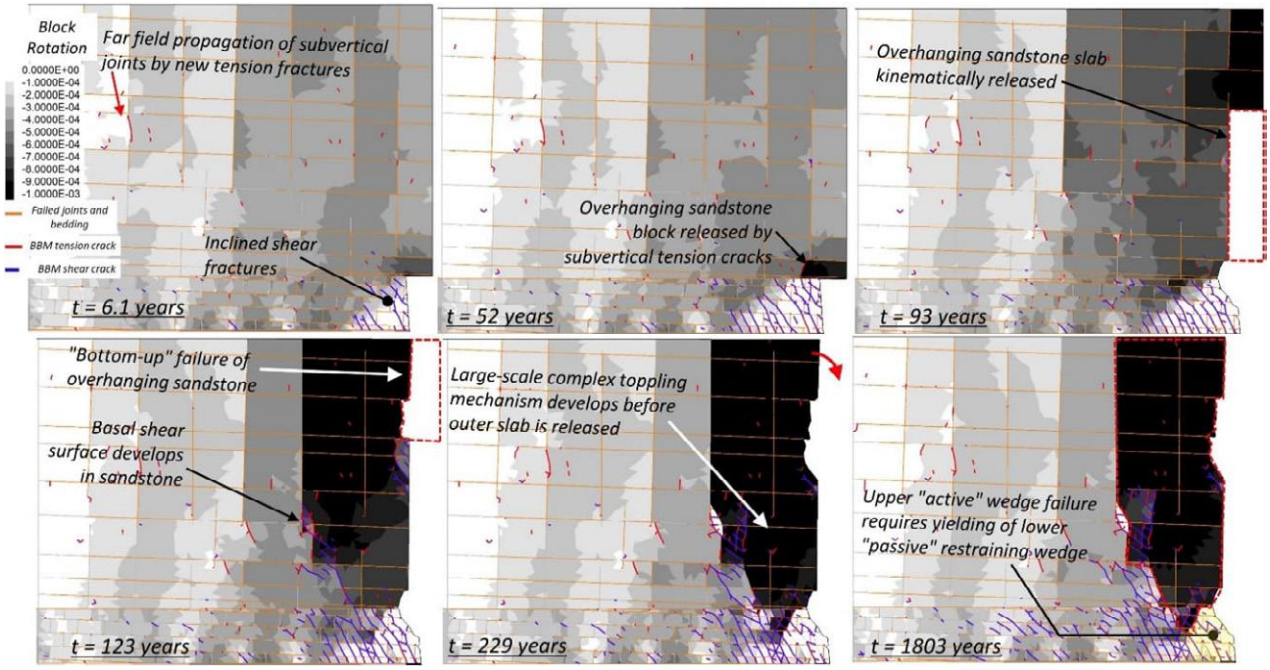

Figure 20: Progressive cliff failure for high *in situ* stress scenario

Figure 21 presents history plots for both stress scenarios, showing (1) subcritical timestep Δt and the maximum stress intensity ratio versus subcritical time; and (2) the rate of brittle failure in terms of the total length of BBM contacts failed in tension and in shear. The crack length histories highlight the main difference between the two scenarios: the lithostatic model records a slow rate of crack growth for the first ~1000 years of subcritical time, followed by a rapid phase of accelerated brittle failure between 1000 and 1200 years. The high stress scenario records rapid shear crack growth from the start of cycling up to approximately 200 years of subcritical time.

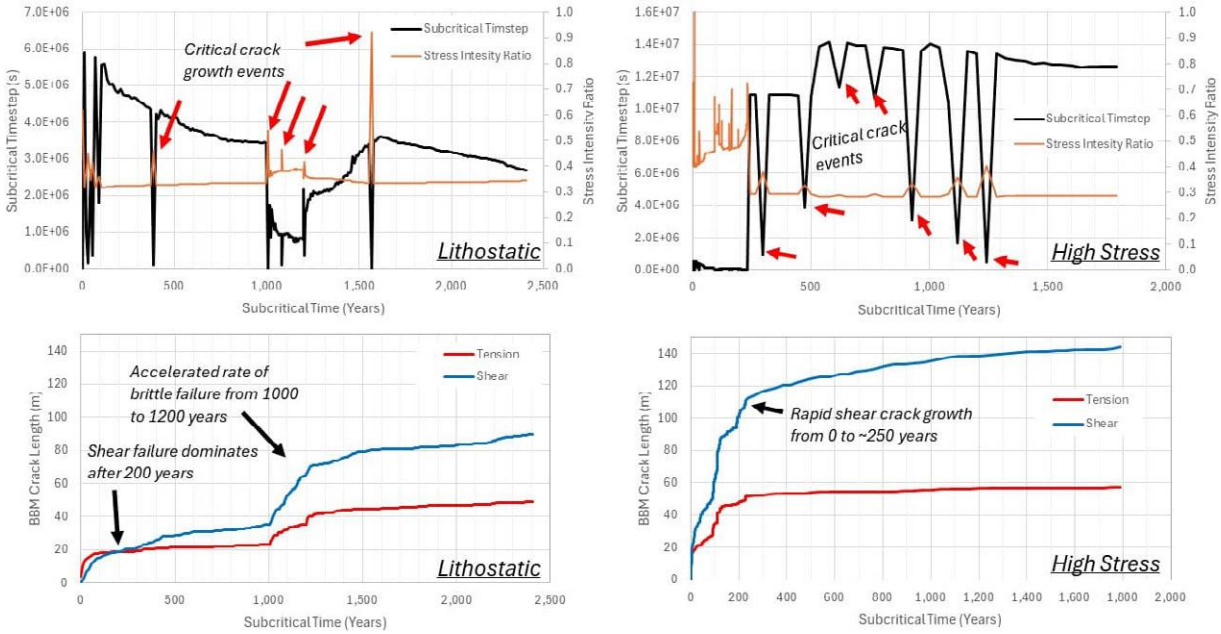

Figure 21: Comparison of subcritical crack data histories for lithostatic and high stress scenarios

The lithostatic scenario is dominated by tensile failure for the first 200 years of subcritical time; this is followed by 800 years of slow progressive failure dominated by subcritical crack growth, until a marked acceleration in BBM contact failure occurs between 1000 and 1200 years, leading to the development of a large scale basal shearing surface that connects through the sandstone rock mass and into the weaker underlying shale. In contrast, the high stress scenario produces an accelerated rate of crack growth, with most damage developing during the first 200 years.

The high stress scenario produces a greater magnitude of displacement at any given timestep. Both simulations suggest that the first block to fail is a thin overhanging slab bounded above by bedding on the immediate "roof" of the overhanging sandstone cliff, with incipient failure developing within the first 10 years of subcritical time. Failure progresses in a "bottom up" process as brittle tension fractures propagate upward, subparallel to the cliff face, releasing newly exposed overhanging sandstone blocks. Large-scale cliff failure involves the development of inclined shear fractures that interact with subvertical joints to allow slabs to detach from the cliff. BBM tensile failure dominates where cracks propagate from the tips of subvertical joints, and shear failure dominates in the basal shale layer.

7 DISCUSSION

The outcrop-scale simulations presented in Section 5 show how intact rock bridges play a critical role in rockfall initiation when failure is controlled by discontinuity propagation. The location of intact rock bridges on the incipient release surface determines their prevailing loading conditions. If rock bridges are subject to tensile loading, failure is controlled by the tensile strength of intact rock and the mode I fracture toughness K_{IC}. In most brittle materials (including rock) K_{IC} is less than the mode II (shear) fracture toughness K_{IIC} and consequently, rock bridges loaded in tension are associated with higher rates of subcritical crack growth. Given two rock bridges of equal size subject to loading in shear and tension respectively, the rock bridge loaded in tension is expected fail first.

For a conceptual 5 m high sandstone slab with a fixed rock bridge content, the time to failure t_f may vary over three orders of magnitude depending on rock bridge geometry. The time to failure versus rock bridge content can be conceptually approximated with power law relationships, such that a marked acceleration in subcritical crack growth occurs when rock bridge content is reduced below 5% to 10% of the slab height. The results demonstrate that relatively small changes in intact rock bridge content have a significant impact on the timescale required for rockfall to initiate. Although it may be impossible to precisely measure the 3D geometry of intact rock bridges occluded inside an outcrop, geotechnical field mapping may be improved with careful attention to the geometry of the specific discontinuities that are expected to control failure kinematics. Measuring the geometry of discontinuity tips that terminate in intact rock may provide a useful indication of apparent intact rock bridge geometry. Classifying the degree of "incipiency" of critical joint sets in terms of their persistence, aperture, and connectivity may provide a useful starting point for estimating the potential cohesion and tensile strength provided by intact rock bridges (Shang et al., 2018).

The cliff-scale simulations presented in Section 6 showed how a subcritical crack growth algorithm can be used to model multi-scale progressive brittle failure driven by undermining. Stress-dependent subcritical crack growth parameters account for the effect of confinement in suppressing crack growth behind the cliff face: the sequence of progressive failure begins with localised brittle fracture near the unconfined cliff face, with progressive release of overhanging blocks in a "bottom up" process as new brittle fractures propagate subparallel to the cliff face.

When the *in situ* stress field is assumed to be lithostatic, brittle crack growth is slow for the first 1000 years of simulated subcritical time. During this phase, localised critical crack growth events involve propagation of subvertical tension cracks in the sandstone unit, and the development of inclined shear cracks in the weaker underlying shale layer. When an anisotropic high horizonal stress field is adopted, crack growth is markedly accelerated, with most of the slope damage (indicated by failed BBM contacts) developing during the first 200 years of subcritical time. In either case, the first rockfalls to release from the cliff are localised metre-scale blocks of sandstone where failure kinematics involve free-fall of wedges or slabs formed by overhanging sandstone beds. Larger overall slope-scale failure requires hundreds to thousands of years of time for the development of a global basal rupture surface.

The cliff-scale modelling suggests that careful consideration must be given to the initial stress conditions and the subcritical timestep Δt. Empirical observations from the Blue Mountains suggest that naturally occurring, large-scale cliff collapse events repeat on a timescale of hundreds to thousands of years. These results suggest that the lithostatic stress model produces a reasonable temporal progression of cliff-scale failure, supporting the hypothesis that the escarpment cliffs have become "de-stressed" over geological time, by the slow removal of horizontal confinement.

8 CONCLUSIONS

This paper has demonstrated how an idealised model for the stress intensity around a coplanar intact rock bridge can be used to simulate time-dependent rockfall initiation controlled by subcritical crack growth. Bonded block discrete element models can represent outcrop-scale or rock mass scale brittle failure processes, using a stress-dependent subcritical timestep and a modified version of the Charles power law that accounts for crack growth under mode I (tensile) and mode II (shear) loading.

The numerical models from this investigation are not calibrated to site-specific slope monitoring data. However, the results demonstrate how the time required for failure to develop can vary depending on *in situ* stress conditions and the geometry of intact rock bridges and pre-existing discontinuities. The order-of-magnitude estimates of time to failure can provide preliminary guidance on the annualised probability of failure used for rockfall risk assessment.

When rock bridge content is less than 5% to 10% of the failure surface, rockfall initiation under gravitational self-weight may occur over tens to hundreds of years, depending on rock bridge geometry. Larger rock mass scale cliff collapse events involve complex interactions between pre-existing discontinuities and brittle fractures that develop in tension and shear, requiring hundreds to thousands of years to propagate and coalesce into a global rupture surface. Future trials of this technique may help to constrain temporal estimates for probability of failure across a broad range of scales and in different geological environments.

CRediT authorship contribution statement

Zack Tuckey: Conceptualisation, Investigation, Writing - original draft.

9 REFERENCES

Alzo'ubi, A.M. (2009). The effect of tensile strength on the stability of rock slopes. PhD thesis, University of Alberta.

Australian Geomechanics Society (AGS) (2007). Practice note guidelines for landslide risk management. *Australian Geomechanics Journal*, 42(1), 63-114.

Backers, T. (2004). Fracture toughness determination and micromechanics of rock under mode I and mode II loading. Doctoral dissertation, University of Potsdam.

Baczynski, N.R.P. (2000). STEPSIM4 "Step-path" method for slope risks. In: *GeoEng 2000*, *Proceedings of the International Conference on Geotechnical and Geological Engineering*, Melbourne.

Bandis, S.C. (2004). Numerical modelling of discrete materials in rock mechanics: developments and engineering applications. In: *Proceedings of the 1st International UDEC/3DEC Symposium*. Bochum, Germany

Bertuzzi, R. and Pells, P.J. (2002). Geotechnical parameters of Sydney sandstone and shale. *Australian Geomechanics: Journal*, 37(5), 41-54.

Call, R.D., and Nicholas, D.E. (1978). Prediction of step path failure geometry for slope stability analysis. In: Proceedings of the 19th US Symposium on Rock Mechanics, Stateline, Nevada; *International Journal of Rock Mechanics and Mining Sciences & Geomechanics Abstracts*, 16(1).

Christianson, M., Board, M. and Rigby, D. (2006). UDEC simulation of triaxial testing of lithophysal tuff. In *ARMA US Rock Mechanics/Geomechanics Symposium*.

Collins, B.D. and Stock, G.M. (2016). Rockfall triggering by cyclic thermal stressing of exfoliation fractures. *Nature Geoscience*, 9(5), 395-400.

Deparis, J., Garambois, S. and Hantz, D. (2007). On the potential of Ground Penetrating Radar to help rock fall hazard assessment: A case study of a limestone slab, Gorges de la Bourne (French Alps). *Engineering Geology*, 94(1-2), 89-102.

Dershowitz, W.S., Lee, G., Geier, J., and LaPointe, P.R. (1998). *FracMan: interactive discrete fracture data analysis, geometric modelling and exploration simulation.* User documentation, Golder Associates Inc., Seattle.

Donati, D., Stead, D. and Borgatti, L. (2023). The influence of slope damage on the kinematics of landslides. *Italian Journal of Engineering Geology and Environment*, 39-47.

Einstein, H.H., Veneziano, D., Baecher, G.B. and O'Reilly, K.J., (1983). The effect of discontinuity persistence on rock slope stability. *International journal of rock mechanics and mining sciences & geomechanics abstracts*, 20(5), 227-236.

Elmo, D., Donati, D. and Stead, D. (2018). Challenges in the characterisation of intact rock bridges in rock slopes. *Engineering Geology*, 245, 81-96.

Fergusson, C. and Hatherly, P. (2023). Segmentation and fault–monocline relationships in the Lapstone Structural Complex, Sydney Basin, New South Wales. *Australian Journal of Earth Sciences*, 70(3), 375–392

Frayssines, M. and Hantz, D. (2006). Failure mechanisms and triggering factors in calcareous cliffs of the Subalpine Ranges (French Alps). *Engineering Geology*, 86(4), 256-270.

Gao, F.Q. and Stead, D. (2014). The application of a modified Voronoi logic to brittle fracture modelling at the laboratory and field scale. *International Journal of Rock Mechanics and Mining Sciences*, 68, 1-14.

Gao, F. (2013). Simulation of failure mechanisms around underground coal mine openings using discrete element modelling. Doctoral dissertation, Simon Fraser University, Department of Earth Sciences.

Guerin, A., Jaboyedoff, M., Collins, B.D., Derron, M.H., Stock, G.M., Matasci, B., Boesiger, M., Lefeuvre, C. and Podladchikov, Y.Y. (2019). Detection of rock bridges by infrared thermal imaging and modeling. *Scientific Reports*, 9(1).

Hatherly, P. (2019). Landscape evolution of the Blue Mountains revealed by longitudinal river profiles and Cenozoic basalts and gravels. *Australian Journal of Earth Sciences*, 67(2), 243-263.

Hatherly, P. and Brown, I. (2022). *The Blue Mountains: Exploring landscapes shaped by the underlying rocks, uplift and erosion*. Windy Cliff Press.

Havaej, M. and Stead, D. (2016). Investigating the role of kinematics and damage in the failure of rock slopes. *Computers and Geotechnics*, 78, 181-193.

Jennings, J.E. (1970). A mathematical theory for the calculation of the stability of slopes in open cast mines. In: *Proceedings of Planning Open Pit Mines*. A.A. Balkema, Cape Town, 87-102.

Kemeny, J. (2003). The time-dependent reduction of sliding cohesion due to rock bridges along discontinuities: a fracture mechanics approach. *Rock Mechanics and Rock Engineering*, 36, 27-38.

Kemeny, J. (2005). Time-dependent drift degradation due to the progressive failure of rock bridges along discontinuities. *International Journal of Rock Mechanics and Mining Sciences*, 42(1), 35-46.

Ko, T.Y. and Kemeny, J. (2011). Subcritical crack growth in rocks under shear loading. *Journal of Geophysical Research: Solid Earth*, 116(B1).

Lee, J.S. (2007). Time-dependent crack growth in brittle rocks and field applications to geologic hazards. PhD Dissertation, University of Arizona.

Mas Ivars, D., Pierce, M.E., Darcel, C., Reyes-Montes, J., Potyondy, D.O., Young, R.P. and Cundall, P.A. (2011). The synthetic rock mass approach for jointed rock mass modelling. *International Journal of Rock Mechanics and Mining Sciences*, 48(2), 219-244.

McMahon, B.K. (1979). *Report to Bougainville Copper Limited on Slope Design Studies*, Pan Hill. McMahon, Burgess and Yeates, Sydney.

Nejati, H.R. and Moosavi, S.A. (2017). A new brittleness index for estimation of rock fracture toughness. *Journal of Mining and Environment*, 8(1), 83-91.

Oliveira, D. (2014). An alternative view on geotechnical parameters for tunnel design in Sydney. *Australian Geomechanics Journal*, 49(3), 95-108.

Oliveira, D., and Parker, C. (2014). An alternative approach for assessing in situ stresses in Sydney. In: *Proceedings of the 15th Australasian Tunnelling Conference*, 189-194. Sydney, NSW, 17-19 September.

Paronuzzi, P. and Serafini, W. (2009). Stress state analysis of a collapsed overhanging rock slab: a case study. *Engineering Geology*, 108(1-2), 65-75.

Sampaleanu, C. (2017). The role of intact rock fracture in rockfall initiation. MSc Thesis, Simon Fraser University.

Scavia, C. (1990). Fracture mechanics approach to stability analysis of rock slopes. *Engineering Fracture Mechanics*, 35(4-5), 899-910.

Shang, J., West, L.J., Hencher, S.R. and Zhao, Z. (2018). Geological discontinuity persistence: Implications and quantification. *Engineering Geology*, 241, 41-54.

Shang, J., Hencher, S.R., West, L.J. and Handley, K. (2017). Forensic excavation of rock masses: a technique to investigate discontinuity persistence. *Rock Mechanics and Rock Engineering*, 50, 2911-2928.

Stead, D., Eberhardt, E. and Coggan, J.S. (2006). Developments in the characterization of complex rock slope deformation and failure using numerical modelling techniques. *Engineering Geology*, 83(1-3), 217-235.

Terzaghi, K. (1962). Stability of steep slopes on hard unweathered rock. *Geotechnique*, 12(4), 251-270.

Tuckey, Z. (2023). The role of progressive brittle fracture in the 1931 landslide at Dogface Rock, Katoomba. *Australian Geomechanics Journal*, 58(3), 77-93.

Wyllie, D.C. and Mah, C. (2005). *Rock slope engineering*, 4th Edition. Taylor & Francis.

Zheng, Y., Chen, C., Liu, T., Zhang, H., Xia, K. and Liu, F. (2018). Study on the mechanisms of flexural toppling failure in anti-inclined rock slopes using numerical and limit equilibrium models. *Engineering Geology*, 237, 116-128.